

# Optical spectra obtained from amorphous films of rubrene: Evidence for predominance of twisted isomer

M. Kytka,<sup>1,2</sup> L. Gisslen,<sup>3</sup> A. Gerlach,<sup>1</sup> U. Heinemeyer,<sup>1</sup> J. Kováč,<sup>2</sup> R. Scholz,<sup>3</sup> and F. Schreiber<sup>1,\*</sup>

<sup>1</sup>*Institut für Angewandte Physik, Universität Tübingen,  
Auf der Morgenstelle 10, 72076 Tübingen, Germany*

<sup>2</sup>*Department of Microelectronics, Slovak University of Technology and  
International Laser Center, Ilkovičova 3, 812 19 Bratislava, Slovakia*

<sup>3</sup>*Walter Schottky Institut, Technische Universität München, Am Coulombwall 3, 85748 Garching, Germany*

(Dated: October 23, 2018)

In order to investigate the optical properties of rubrene we study the vibronic progression of the first absorption band (lowest  $\pi \rightarrow \pi^*$  transition). We analyze the dielectric function  $\epsilon_2$  of rubrene in solution and thin films using the displaced harmonic oscillator model and derive all relevant parameters of the vibronic progression. The findings are supplemented by density functional calculations using B3LYP hybrid functionals. Our theoretical results for the molecule in two different conformations, i.e. with a twisted or planar tetracene backbone, are in very good agreement with the experimental data obtained for rubrene in solution and thin films. Moreover, a simulation based on the monomer spectrum and the calculated transition energies of the two conformations indicates that the thin film spectrum of rubrene is dominated by the twisted isomer.

## I. INTRODUCTION

Organic semiconductors have become very promising and actively investigated materials [1, 2, 3]. Due to their specific optical properties organic molecules are particularly interesting for various device applications such as light emitting diodes, field effect transistors and solar cells [4, 5, 6]. Different studies have demonstrated that the optical properties of molecular solids are strongly influenced by their structure. Crystalline materials as for example pentacene [7] and diindenoperylene [8] thin films exhibit complex and generally anisotropic absorption spectra which are often influenced by characteristic charge transfer excitations. Amorphous materials with extended  $\pi$ -conjugated electron systems, as for example rubrene (Fig. 1), show optical spectra which are seemingly simpler to understand [9, 10, 11]. However, when considered in more detail the growth of amorphous materials may present its own complications. For example, studies of rubrene thin films on silicon uncovered a surprising growth behavior: Using X-ray reflectivity rubrene thin films are found to be relatively smooth and amorphous over a large thickness range [11]. Yet, an anomalous roughness evolution of the films is observed, i.e. a decrease of the film roughness at the beginning (below  $\sim 20$  nm) and a subsequent increase of the roughness at a later stage. Recent near edge X-ray absorption fine structure (NEXAFS) results indicate the existence of different rubrene isomers on  $\text{SiO}_2$  and  $\text{Au}(111)$  [10]. At the early stage of growth both species were identified, i.e. the rubrene with the twisted and planar tetracene backbone, followed by the planar isomer only.

In the present study we focus on the optical proper-

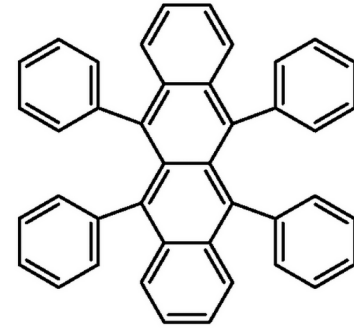


FIG. 1: Structure of the rubrene molecule ( $\text{C}_{42}\text{H}_{28}$ ) which consists of a tetracene backbone (TBB) and four attached phenyl rings. Due to the different orientation of the phenyl rings and TBB the  $\pi$ -conjugated systems of both parts are strongly decoupled.

ties of rubrene molecules in solution and amorphous thin films. In particular, we investigate whether the different isomers can be identified in the optical spectra. For this purpose we calculate the optical response of the different isomers of rubrene with time-dependent density functional theory (TD-DFT). The deformation in the relaxed excited geometry of each isomer found with TD-DFT is projected onto its internal vibrations. This allows an assignment of the observed sub-bands in the absorption spectra to an effective vibrational mode which is an average over the various internal vibrations elongated in the relaxed excited geometry. Furthermore, we use the calculations to assess the contribution of the different rubrene isomers to the observed spectra.

\*Electronic address: frank.schreiber@uni-tuebingen.de

## II. EXPERIMENT

The material used in our experiments was purchased from Acros and purified by gradient sublimation. This procedure yields small rubrene crystallites which are relatively inert against oxidation in air [9]. To avoid well-known thermochromic effects – rubrene changes its color towards the red at elevated temperatures [12] – we took all spectra at  $T = 25^\circ\text{C}$ .

The absorption spectra of rubrene in acetone solution were recorded using a UV-Vis spectrophotometer (Varian Cary 50). With an overall reproducibility of the optical constants being on a 1% level we verified that for the chosen concentrations ( $1.46 \times 10^{-5} - 1.15 \times 10^{-4}$  mol/l) the absorbance data follow the Lambert-Beer law. The optical properties of rubrene thin films were measured in ultra-high vacuum using a spectroscopic rotating compensator ellipsometer (Wollam M-2000) with a broad band 75 W Xe lamp (250 – 1000 nm) and CCD based detection system with a spectral resolution of about 1.6 nm. The organic material was out-gassed in vacuum for several days at  $\sim 190^\circ\text{C}$  in order to remove residual rubrene peroxide [13]. Well cleaned Si(100) substrates with a thermal oxide layer (thickness  $\sim 20$  nm) were transferred into the growth chamber and kept at temperatures above  $400^\circ\text{C}$  for several hours. Before deposition of the organic material we determined the thickness of the silicon oxide and the precise angle of incidence by ellipsometry. The rubrene films were deposited at room temperature via sublimation from a Knudsen cell at  $210^\circ\text{C}$ . A typical deposition rate of 0.2 nm/min and a pressure of less than  $1 \times 10^{-9}$  mbar during growth ensured reproducible results.

The experimental data were analyzed with the commercial WVASE software package [14]. Since rubrene grows in amorphous films, we used an isotropic model consisting of three layers, i.e. rubrene – silicon dioxide – silicon, with the optical constants of silicon and silicon dioxide taken from Ref. [15]. First, we determined the thickness of the rubrene film by employing a Cauchy model in the spectral range below 2 eV, where the absorption of the organic material is negligible. Then, we performed a point-by-point fit which yields the complex dielectric constant  $\varepsilon_1 + i\varepsilon_2$  for each energy, see Fig. 2(a,b). To check the Kramers-Kronig consistency of the optical constants we also analyzed the experimental data with a general oscillator model. In this approach the imaginary part of the dielectric function  $\varepsilon_2$  is described by a sum of Gaussian peaks and the real part  $\varepsilon_1$  is derived by the Kramers-Kronig relation. Generally, we found excellent agreement of the results obtained either by point-by-point fits or the general oscillator model. To check the consistency of the results obtained by UV-Vis spectroscopy and spectroscopic ellipsometry we also measured transmission spectra of rubrene on glass, see Fig. 2c. We found that these data can be described very well using the optical constants of rubrene on silicon obtained by ellipsometry (and those of glass measured sep-

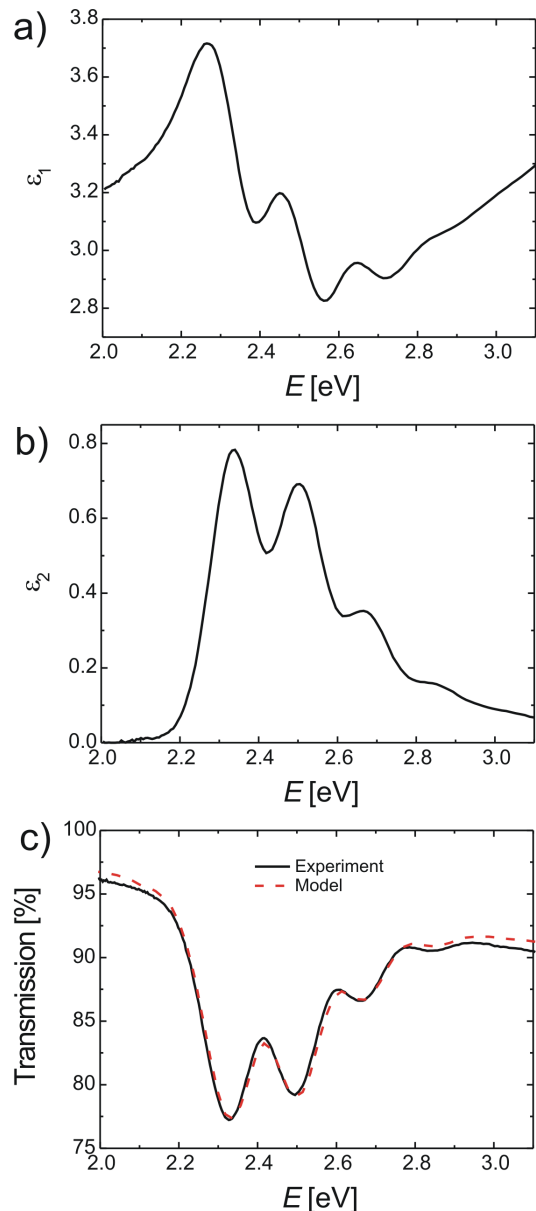


FIG. 2: (Color online) Complex dielectric function of a 33 nm thick rubrene film on  $\text{SiO}_2$ . (a) Real part  $\varepsilon_1$  and (b) Imaginary part  $\varepsilon_2$ . The optical properties were obtained *in situ* by spectroscopic ellipsometry and analyzed using a point-by-point fit. (c) Light transmission through a 34 nm thick rubrene film on glass measured in air (solid black). A model, which is based on the optical constants of rubrene shown above (a, b) and the optical constants of glass obtained separately by variable angle spectroscopic ellipsometry, can be used to describe the data (dashed red).

arately with variable angle ellipsometry). The minor differences between the data and the model might be due to oxidation of some rubrene molecules in air [16, 17].

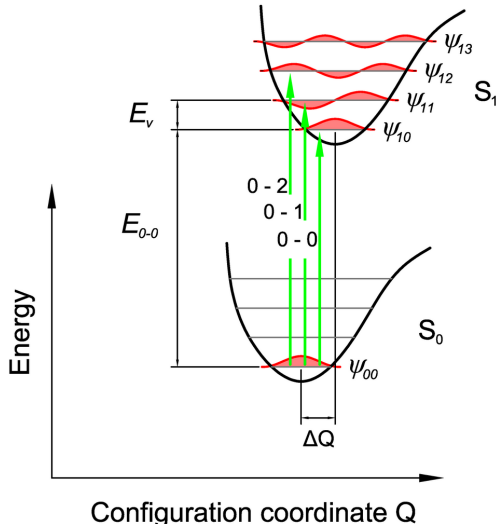


FIG. 3: (Color online) Displaced harmonic oscillator model. Because of different electron configurations in the  $S_0$  (HOMO) and the  $S_1$  (LUMO) electronic excitations result in spatial deformations of the molecule. The corresponding change of the configurational coordinate  $Q$  gives rise to the observed vibronic excitations.

### III. RESULTS

#### A. Analysis of the optical spectra

The imaginary part of the dielectric function (Fig. 2b) shows a pronounced vibronic progression with five clearly distinguishable sub-bands. The displaced harmonic oscillator model – a simplified scheme describing the dipole-allowed transitions between the electronic ground state ( $S_0$ ) and the first excited state ( $S_1$ ) including spatial deformations of the molecule (Fig. 3) – has been used to model the data. In this approximation the excitation energies  $E_n$  are given by

$$E_n = E_{0-0} + nE_v, \quad (1)$$

where  $E_{0-0}$  is the energy of the  $S_{00} \rightarrow S_{10}$  transition,  $E_v$  the vibrational energy and  $n$  the vibrational quantum number of the excited state. The intensities  $I_n$  of the vibronic sub-bands contribute to the imaginary part of the dielectric function according to a Poisson progression

$$I_n = I \frac{S^n}{n!} e^{-S}, \quad (2)$$

where  $S$  is the electron-phonon coupling constant, also known as the Huang-Rhys factor. This coupling parameter essentially determines the shape of the absorption spectrum, i.e. the relative intensities  $I_n$  of the vibronic sub-bands, which are given by the area under each peak.

In order to compare the data taken in solution with the thin film spectra the absorption coefficient  $\alpha$  of the solution has been converted to the dielectric function using the common approximation that the refractive index

is virtually constant towards high energies and  $\varepsilon_2$  is then proportional to  $\alpha/E$ . Fig. 4a shows the normalized data for rubrene in acetone solution and thin films together with the corresponding least-square fits.

With the sub-band energies given by Eq. (1), their relative intensities  $I_n$  according to the Poisson progression in Eq. (2), and a Gaussian for each sub-band, the imaginary part of the dielectric response can be expressed as

$$\varepsilon_2(E) = \sum_{n=0}^5 \frac{I_n}{\sigma_n \sqrt{2\pi}} \exp \left[ -\frac{(E - E_n)^2}{2\sigma_n^2} \right], \quad (3)$$

where the broadening parameters  $\sigma_n$  are related to the respective widths of each sub-band by  $\text{FWHM}_n = \sqrt{8 \ln 2} \sigma_n$ . Since several internal modes might contribute to each sub-band, the linewidth are not necessarily constant. In the fitting algorithm all parameters except the width of the last two peaks (fixed at  $\sigma_4 = 0.08$  eV and  $\sigma_5 = 0.1$  eV) have been varied. The Huang-Rhys factor  $S$  is then deduced from the intensities of the first four transition peaks using Eq. (2), see Fig. 4b [27]. The results of the fitting procedure for the vibronic progression are summarized in Tab. I.

	$E_{0-0}$	$E_v$	$S$
Solution	2.359	0.165	0.986
Thin Film	2.335	0.169	0.974

TABLE I: Parameters derived from the experimental data using the model of the displaced harmonic oscillator for rubrene in acetone solution and thin films: transition energy between the vibrational ground states  $E_{0-0}$  (eV), vibrational energy  $E_v$  (eV) and Huang-Rhys factor  $S$ .

#### B. DFT calculations

In order to study the effect of possible conformational changes of the molecule and to compare the experimental results with theory we have computed the excitation energies and the deformation in the lowest excited state of rubrene using the TURBOMOLE 5.7 program package [18]. We have chosen the B3LYP hybrid functional since it gives excellent molecular geometries of organic molecules together with rather precise transition energies resulting from a compensation between the systematic deviations arising from the underlying gradient-corrected density functional and the Hartree-Fock contribution [19]. For the electronic orbitals, we use a triple- $\zeta$  valence polarized (TZVP) basis [20] throughout this article.

In order to cover the twisted and the planar isomers of rubrene, we have optimized both of them in their respective point groups, i.e.  $D_2$  for the twisted isomer, and  $C_{2h}$  for the planar one, see Fig. 5. Our simulation reproduces the known fact that the twisted isomer is more stable [10], with an energetic difference of 0.172 eV at the B3LYP/TZVP level.

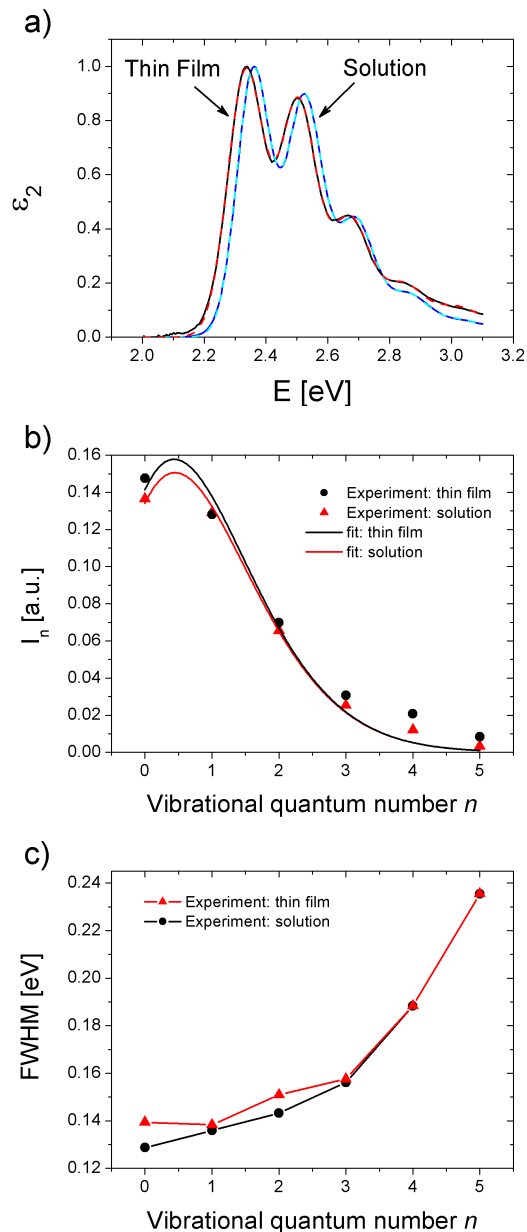


FIG. 4: (Color online) (a) Normalized dielectric function  $\epsilon_2$  of a 33 nm thick rubrene film (solid black) and of a dilute solution of rubrene in acetone (solid dark blue) with a fit to the data (dashed, red and light blue) based on Eq. (3). The absorption spectrum shows a redshift which is caused primarily by the refractive index of the environment ('solvent shift'). (b) Least-square fit to the intensities  $I_n$  of the vibronic progression using an interpolation of Eq. (2) which yields the Huang-Rhys factors  $S$  for the thin film and the monomer. (c) The width (FWHM) of the transitions peaks. In case of the solution it shows a monotonic increase, which indicates that several vibrational modes contribute to each sub-band.

In solution the charge distribution of the solute molecule polarizes the medium surrounding it, resulting in a further stabilization energy. This phenomenon can be handled with the conductor-like screening model (COSMO), where the solute is treated as lying inside a cavity surrounded by the polarizable medium [21]. In this approach, the response of the dielectric medium is replaced by an ideal conductor, generating screening charges on the surface of the cavity. In a second step these screening charges are scaled by a factor  $f$  depending on the dielectric constant  $\epsilon$  of the solvent,  $f(\epsilon) = (\epsilon - 1)/(\epsilon + \frac{1}{2})$ . We have applied the respective routine as implemented in the TURBOMOLE 5.7 program package to a geometry optimization of each isomer in a medium with a dielectric constant of  $\epsilon = 20.7$  corresponding to acetone. At the B3LYP/TZVP level we found stabilization energies of 0.312 eV for the planar isomer, and 0.303 eV for the twisted isomer. This is reducing the energetic difference between the two isomers by a small amount, but the twisted isomer still remains more stable by 0.163 eV.

Even though the twisted isomer is more stable both as a free molecule and in solution, in the crystalline phase the planar isomer can be stabilized by a beneficial geometric arrangement between neighboring molecules, resulting in a large cohesive energy so that the energetic cost of the planarization is overcompensated by attractive inter-molecular interactions. In the amorphous phase of solid rubrene it is expected that the twisted geometry is conserved because the random positions and orientations of the neighboring molecules cannot stabilize an unfavorable isomer.

The different energies of both isomers raise the question if the planar isomer is stable, or if it can spontaneously transform into the more favorable twisted geometry. Using B3LYP and basis sets in the size range between 6-31G(d) and TZVP we found that the lowest symmetry-breaking  $A_u$  mode in the  $C_{2h}$  point group received a small imaginary frequency. For the larger TZVP basis this apparent instability was found to depend on the integration grid: A calculation using the standard  $m3$  grid resulted in an imaginary frequency of  $i13 \text{ cm}^{-1}$ , but based on a denser  $m4$  grid, this value decreased towards  $i5 \text{ cm}^{-1}$ . Using a tighter convergence of  $10^{-8}$  Hartree, the energetic minimum along this imaginary mode occurs at  $12 \text{ cm}^{-1} = 1.5 \text{ meV}$  below the  $D_2$ -symmetric isomer. However, independently of basis size and integration grid, for larger deformations along this vibrational eigenvector, the shape of the potential returns to an essentially parabolic minimum, with a tiny distortion for small deformations. Hence, this ultra-soft or even imaginary mode does not constitute a viable barrierless pathway from the planar isomer to the twisted configuration. For the twisted isomer we found positive frequencies for all vibrational modes, the lowest being a breathing mode at  $26 \text{ cm}^{-1}$ .

In the twisted isomer the repulsion between the phenyl side groups achieves a rather larger distance between

them as opposed to the planar isomer, where a relatively small distance between the phenyl groups is enforced by the rigidity of the bond connecting each side group to the tetracene core and by the more restrictive point group  $C_{2h}$ . Therefore, the twisted isomer gains a substantial amount of energy through a reduction of these repulsive interactions, allowing eventually to invest a part of this energy into the unfavorable twist of the tetracene backbone. The resulting angle between the two central rings of the tetracene core is  $22.8^\circ$  in the electronic ground state, and the angle between the two final rings  $42.0^\circ$ , compare Fig. 5b. In the relaxed excited state these angles increase to  $26.7^\circ$  and  $43.6^\circ$ , respectively.

For both isomers the relaxed excited geometries are computed with time-dependent density functional theory (TD-DFT) at the B3LYP/TZVP level, conserving in each case the point group of the electronic ground state. The resulting deformation pattern is projected onto the symmetry-conserving breathing modes of the respective isomer in its ground state, defining in turn a Huang-Rhys  $S_j$  factor for each vibration  $\hbar\omega_j$ . In contrast to the lowest symmetry-breaking vibration of the planar isomer the frequencies of the symmetry-conserving modes depend only weakly on variational basis set and integration grid, with the largest influence for the lowest breathing mode found at  $19\text{ cm}^{-1}$  (B3LYP/TZVP,  $m3$ ) or  $22\text{ cm}^{-1}$  (B3LYP/TZVP,  $m4$ ). Correspondingly, we have determined similar values for the Huang-Rhys factors obtained at these levels. Applying the projection scheme to the deformation pattern of a cationic molecule, we have reproduced the key features of previous calculations addressing the Huang-Rhys factors in the planar isomer [22]. Of course, when compared to the cationic geometry, a neutral excitation of a planar rubrene molecule produces a somewhat different set of Huang-Rhys factors.

By averaging over vibrations in the range between  $900$  and  $1800\text{ cm}^{-1}$  we define an *effective mode* with a Huang-Rhys factor  $S_{\text{eff}} = \sum_j S_j$ , a reorganization energy  $\lambda_{\text{eff}} = \sum_j S_j \hbar\omega_j$ , and a mode energy of  $\hbar\omega_{\text{eff}} = \lambda_{\text{eff}}/S_{\text{eff}}$ . The harmonic approximation to the potential energy surface results in slightly too large vibrational frequencies. In order to compensate for this deviation we apply a scaling factor of  $0.973$  adequate for the B3LYP functional to the vibrational frequencies [23, 24], conserving however the reorganization energies  $\lambda_j$  assigned to each mode, so that the Huang-Rhys factors are increased by a factor of  $1.028 = 1/0.973$ . The results of this computational procedure are reported in Tab. II. We use two kinds of relaxed excited geometries: First, the result of the TD-DFT geometry optimization, and second, a modified excited geometry where changes of the twisting angle of each phenyl group around the bond connecting it to the tetracene core are eliminated. From similar investigations on other molecules containing phenyl groups we expect that this procedure minimizes artifacts arising from finite angle effects related to the relatively large changes of these angles in the relaxed excited geometry [25].

When basing our projection directly onto the TD-DFT

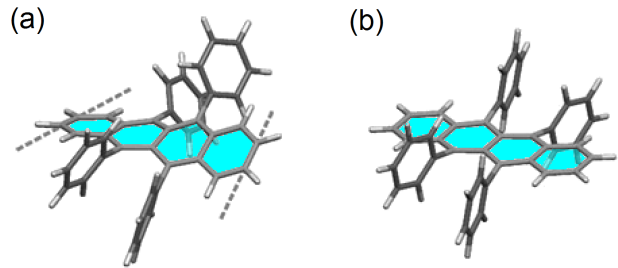


FIG. 5: (Color online) (a) Geometry of the most stable rubrene isomer with a twisted tetracene backbone, and (b) planar rubrene isomer, which resembles the geometry in the crystalline phase.

geometry for the excited state, the sum over the reorganization energies assigned to each mode exceeds the available reorganization energies  $\lambda^{(g)}$  and  $\lambda^{(e)}$  deduced from the potential energy surfaces of ground and excited state, respectively. Using instead the modified excited state geometry where the orientation of the phenyl groups is adjusted to the ground state geometry, this artifact disappears, indicating that the non-orthogonality problems arising from the modified orientation of the phenyl rings are eliminated. Moreover, in the second projection scheme the frequency assigned to the effective mode is in better agreement with the observations.

	twisted	planar
$E_{\text{abs}}$	2.173	2.279
$E_{0-0}$	1.965	2.085
$\lambda^{(g)}$	0.204	0.195
$\lambda^{(e)}$	0.208	0.194
$\hbar\omega_{\text{eff}}$ (TD-DFT)	0.155	0.150
$S_{\text{eff}}$ (TD-DFT)	1.216	1.358
$\hbar\omega_{\text{eff}}$ (no twisting)	0.162	0.158
$S_{\text{eff}}$ (no twisting)	0.985	1.025

TABLE II: Vertical transition energy  $E_{\text{abs}}$  (eV) in the ground state geometry, transition energy between lowest vibrational levels  $E_{0-0}$  (eV), reorganization energies  $\lambda^{(g)}$  (eV) and  $\lambda^{(e)}$  (eV) on ground and excited state potential energy surfaces, respectively, effective mode  $\hbar\omega_{\text{eff}}$  (eV), and effective Huang-Rhys factor for the twisted and planar isomers of rubrene, before (TD-DFT) and after (no twisting) eliminating the influence of a modified orientation of the phenyl side groups in the relaxed excited geometry. All B3LYP vibrational frequencies are scaled down by a factor of  $0.973$ , and the Huang-Rhys factors  $S$  are scaled up correspondingly by a factor of  $1/0.973 = 1.028$ , so that the reorganization energies are conserved. All calculations have been performed at the B3LYP/TZVP level.

#### IV. DISCUSSION

The spectra of rubrene in solution and rubrene thin films show a pronounced vibronic progression that we have analyzed using the displaced harmonic oscillator model. For evaluation of the results the parameters compiled in Tab. I should be compared with each other and with previous investigations: We find that the transition energy  $E_{0-0} = 2.359$  eV of rubrene in acetone solution deviates less than 2 meV from a value reported earlier [26]. Based on the systematic study of solvent shifts presented in that work one can estimate that the HOMO-LUMO transition of rubrene dissolved in acetone is red-shifted by about 0.100 eV with respect to a free molecule. Consequently, the lowest vibronic sub-band in the free molecule would be found at 2.459 eV. This illustrates that the transition energy  $E_{0-0} = 2.335$  eV measured for rubrene in thin films shows a significant redshift which is caused by the environment. Since the Huang-Rhys factors for rubrene monomers dissolved in acetone and amorphous thin films show only minor differences, i.e.  $S_{\text{sol}} = 0.986$  and  $S_{\text{film}} = 0.974$ , we conclude that the exciton-phonon coupling is not markedly influenced by aggregation of the molecules – most likely because the investigated thin films are amorphous and the phenyl side groups keep those neighboring tetracene backbones apart that are mainly involved in the  $\pi \rightarrow \pi^*$  transition.

Furthermore, we observe a continuous increase of the peak width in the vibronic progression of rubrene which indicates that more than one vibrational mode is involved. For the solution spectrum we find a simple monotonic dependency, whereas the thin film spectrum shows a different behavior with the width of the first peak being larger than the second one. One could speculate that this observation is related to the reported existence of a conformational rubrene isomer with a slightly different electronic transition energy [10]. In order to verify whether two different isomers contribute to the optical spectra one might compare the experimental data with the results of the DFT calculations for the twisted and planar molecule (Tab. II): Despite the excellent agreement of the calculated Huang-Rhys factors with our experimental values [28] their small difference ( $S_{\text{twist}} = 0.985$ ,  $S_{\text{plan}} = 1.025$ ) cannot provide the required sensitivity to distinguish both isomers. Our calculations, however, show that the transition energies of the twisted and planar monomer differ significantly with  $\Delta E_{0-0} = 0.120$  eV. Unlike spectra of the pure isomers a mixture of the two molecules therefore would have to show some unusual spectral features.

Based on the solution spectrum of rubrene, which itself represents the twisted isomer, we also model the spectrum of the planar isomer by blue shifting the spectrum by 0.12 eV. By adding both spectra with different weights and normalizing them we simulate a corresponding mixture of planar and twisted molecules, see Fig. 6. We find that the spectrum changes mainly in the low-energy range when the number of twisted molecules is increased

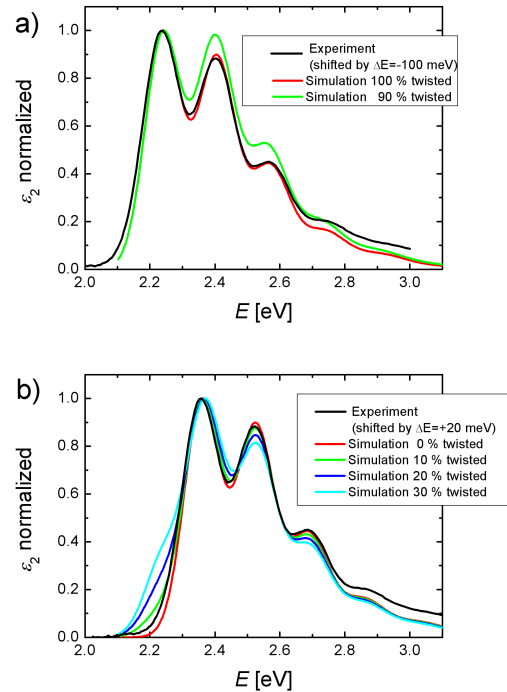


FIG. 6: (Color online) Simulation of the spectra for different mixing ratios of planar and twisted rubrene isomers. To compensate the solvent shift and to allow a comparison of the line shapes the thin film spectrum is shifted in energy such that the  $E_{0-0}$  energy agrees with the simulated spectra. (a) mainly twisted isomers (b) mainly planar isomers.

from e.g. 10 to 30% (Fig. 6b), whereas in the other case increasing the number of planar molecules from 0 to 10% affects mainly the high-energy range (Fig. 6a). Overall the simulations indicate that a contribution of the second rubrene isomer is relative small, i.e. below 10%. Because the twisted isomer is energetically favorable we conclude that the thin film spectrum is dominated by the twisted molecule and a fraction of no more than 10% of planar molecules may contribute to the spectrum. The differences between the solution and the thin film spectrum in the high-energy range, however, cannot be explained by contributions of a small fraction of planar molecules alone. Additional coupling in the thin film, like exciton transfer, might be the origin of this deviation.

#### V. SUMMARY AND CONCLUSIONS

The optical spectra of rubrene thin films and monomers in solution have been investigated experimentally by spectroscopic ellipsometry and UV-Vis spectroscopy. The analysis of the vibronic progression using the displaced harmonic oscillator model has revealed the subtle differences between the monomer and the thin film spectrum. Additionally, time-dependent DFT calculations have been performed for the planar and the twisted

isomer in order to get more insight into possible conformational changes of the molecule as they are known from the literature. The theoretical results, notably the excitation energies and Huang-Rhys parameters for the planar and twisted molecule, are in excellent agreement with the experimental data. Since the two rubrene isomers show different transition energies, the optical spectra may reveal their existence. In fact a simulation, which studies the effect of mixing the two species, indicates that one isomer – most likely the more stable twisted isomer – dominates the thin film spectrum with a percentage of more than 90%.

## Acknowledgments

The authors thank J. Pflaum for purifying rubrene, A. Mateasik for making the UV-Vis spectrometer available and G. Witte for discussing the results of our work. We gratefully acknowledge financial support by DFG, EPSRC, DAAD, Center of Excellence CENAMOST No. VVCE-0049-07 with support of project APVV-0290-06, VEGA 1/0689/09 and computational resources at LRZ Garching.

- 
- [1] W. E. Brütting, *Physics of Organic Semiconductors* (Wiley-VCH, Weinheim, 2005).
- [2] G. Witte and C. Wöll, *Phys. Stat. Sol. (a)* **205**, 497 (2008).
- [3] A. Gerlach, S. Sellner, S. Kowarik, and F. Schreiber, *Phys. stat. sol. (a)* **205**, 461 (2008).
- [4] S.-W. Park, J. M. Hwang, J.-M. Choi, D. K. Hwang, M. S. Oh, J. H. Kim, and S. Im, *Appl. Phys. Lett.* **90**, 153512 (2007).
- [5] S.-W. Park, S. H. Jeong, J.-M. Choi, J. M. Hwang, J. H. Kim, and S. Im, *Appl. Phys. Lett.* **91**, 033506 (2007).
- [6] C. H. Hsu, J. Deng, C. R. Staddon, and P. H. Beton, *Appl. Phys. Lett.* **91**, 193505 (2007).
- [7] A. Hinderhofer, U. Heinemeyer, A. Gerlach, S. Kowarik, R. M. J. Jacobs, Y. Sakamoto, T. Suzuki, and F. Schreiber, *J. Chem. Phys.* **127**, 194705 (2007).
- [8] U. Heinemeyer, R. Scholz, L. Gisslén, M. I. Alonso, J. O. Ossó, M. Garriga, A. Hinderhofer, M. Kytka, S. Kowarik, A. Gerlach, et al., *Phys. Rev. B* **78**, 085210 (2008).
- [9] D. Käfer and G. Witte, *Phys. Chem. Chem. Phys.* **7**, 2850 (2005).
- [10] D. Käfer, L. Ruppel, G. Witte, and C. Wöll, *Phys. Rev. Lett.* **95**, 166602 (2005).
- [11] S. Kowarik, A. Gerlach, S. Sellner, F. Schreiber, J. Pflaum, L. Cavalcanti, and O. Kononov, *Phys. Chem. Chem. Phys.* **8**, 1834 (2006).
- [12] A. Schönberg, A. Mustafa, and W. Asker, *J. Am. Chem. Soc.* **76**, 4134 (1954).
- [13] H. H. Wasserman, J. R. Scheffer, and J. L. Cooper, *J. Am. Chem. Soc.* **94**, 4991 (1972).
- [14] J. A. Woollam (2005).
- [15] C. M. Herzinger, B. Johs, W. A. McGahan, J. A. Woolam, and W. Paulson, *J. Appl. Phys.* **83**, 3323 (1998).
- [16] O. Mitrofanov, D. V. Lang, C. Kloc, J. M. Wikberg, T. Siegrist, W.-Y. So, M. A. Sergent, and A. P. Ramirez, *Phys. Rev. Lett.* **97**, 166601 (2006).
- [17] M. Kytka, A. Gerlach, F. Schreiber, and J. Kováč, *Appl. Phys. Lett.* **90**, 131911 (2007).
- [18] R. Ahlrichs, M. Bär, H. Häser, H. Horn, and C. Kölmel, *Chem. Phys. Lett.* **162**, 165 (1989).
- [19] C. W. Bauschlicher, *Chem. Phys. Lett.* **246**, 40 (1995).
- [20] A. Schäfer, C. Huber, and R. Ahlrichs, *J. Chem. Phys.* **100**, 5829 (1994).
- [21] A. Klamt and G. Schüürmann, *J. Chem. Soc. Perkin Trans.* **2**, 799 (1993).
- [22] D. A. da Silva Filho, E.-G. Kim, and J.-L. Brédas, *Adv. Mater.* **17**, 1072 (2005).
- [23] A. P. Scott and L. Radom, *J. Phys. Chem.* **100**, 16502 (1996).
- [24] M. D. Halls, J. Velkovski, and H. B. Schlegel, *Theo. Chem. Acc.* **105**, 413 (2001).
- [25] R. Scholz, L. Gisslén, C. Himcinschi, I. Vragogić, E. M. Calzado, E. Louis, E. S. F. Maroto, and M. A. Díaz-García, *J. Phys. Chem. A* **113**, 315 (2009).
- [26] G. M. Badger and R. S. Pearce, *Spectrochim. Acta* **4**, 280 (1951).
- [27] In principle, the Huang-Rhys parameter can be derived already from the intensities of only two adjacent peaks. Our approach, however, is more robust and therefore gives reliable results.
- [28] The fact that the calculated Huang-Rhys factor for the twisted isomer nearly coincides with the observed value is accidental: For other applications of the same functional and basis set to the relaxed excited geometry of polyaromatic molecules larger deviations are found.